Research Article

Abdeliazim Mustafa Mohamed*, Majed A. A. Aldahdooh, Bassam A. Tayeh, Maaz Osman Bashir and Yazan Issa Abu Aisheh

Experimental and RSM-based optimization of sustainable concrete properties using glass powder and rubber fine aggregates as partial replacements

https://doi.org/10.1515/rams-2025-0185
Received February 16, 2025; accepted November 19, 2025;
published online December 25, 2025

Abstract: To promote sustainability in concrete production, this study investigates the combined use of glass powder (GP) and rubber fine aggregates (RF) as partial replacements for cement and natural fine aggregates (NF), respectively. The study aligns with several Sustainable Development Goals (SDGs). Ten mixtures were developed using Central Composite Design (CCD) within the Response Surface Methodology (RSM) framework, with GP and RF replacement levels ranging from 0 % to 35 %. Replacing cement with 15 % GP improved compressive strength, tensile strength, and stiffness due to pozzolanic reactivity and packing effects, while higher levels (25–35 %) reduced performance because of increased water demand and dilution. RF replacement up to 15 % maintained workability and strength; beyond this, mechanical properties declined due to RF's low specific gravity (1.06 g/cm^3), weak bonding, and higher porosity. The optimal mix, GP15RF15, achieved a slump of 92 mm, 28-day compressive strength of 40.1 MPa, tensile strength of 5.3 MPa, and modulus of elasticity of 25,914.5 MPa, comparable to the control mix. Correlation analysis showed strong positive relationships among compressive strength, tensile strength, and stiffness ($r \geq 0.99$), while RF content had strong negative correlations ($r = -0.75$ to -0.77). Optimization using the desirability function yielded a score of 1.000, with prediction errors below 1.35 %. The results confirm the viability of GP–RF concrete as a durable and eco-efficient alternative for non-prestressed structural components and general infrastructure.

Keywords: glass waste powder; rubber waste; sustainable concrete; response surface methodology; sustainable development goals (SDGs); mechanical properties

***Corresponding author: Abdeliazim Mustafa Mohamed**, Department of Civil Engineering, College of Engineering in Al-Kharj, Prince Sattam Bin Abdulaziz University, Al-Kharj, 11942, Saudi Arabia,
E-mail: a.bilal@psau.edu.sa
Majed A. A. Aldahdooh, Department of Facilities and Construction Project Management, International College of Engineering and Management, University of Central Lancashire (UK), P.C. 111, Muscat, Oman,
E-mail: majidaldahdooh@icem.edu.om
Bassam A. Tayeh, Civil Engineering Department, Faculty of Engineering, Islamic University of Gaza, P.O. Box 108, Gaza Strip, Palestine; and Department of Civil & Environmental Engineering, University of Waterloo, Waterloo, ON, Canada, E-mail: btayeh@iugaza.edu.ps
Maaz Osman Bashir, Department of Civil Engineering, Faculty of Engineering Sciences, Omdurman Islamic University, Khartoum, Sudan,
E-mail: Maaz.osman122@gmail.com
Yazan Issa Abu Aisheh, Hourani Center for Applied Scientific Research (HCASR), Al-Ahliyya Amman University, Postal Address 19328, Amman, Jordan, E-mail: yabueisheh@hotmail.com. https://orcid.org/0000-0002-9386-0610

Abbreviations

GP	glass powder
RF	rubber fine aggregates
NF	natural fine aggregates
OPC	ordinary Portland cement
RSM	response surface methodology
CCD	central composite design
SCM	supplementary cementitious material
XRF	X-ray fluorescence
CA	coarse aggregates
SP	superplasticizer
[OPC-GP]% (X_1)	replacement level of cement with glass powder (%)
[NF-RF]% (X_2)	replacement level of natural fine aggregates with rubber fine aggregates (%)

1 Introduction

Concrete is a widely used material in modern construction and is primarily valued for its high compressive strength. However, its inherent brittleness and limited tensile capacity remain major drawbacks for structural applications [1, 2]. With growing emphasis on sustainable construction practices, incorporating recycled and industrial waste materials into concrete has become a practical approach to minimizing the environmental impact of conventional production [3, 4]. Among these materials, glass powder (GP), used as a partial cement replacement, and rubber fine aggregates (RF), applied as a substitute for natural fine aggregates (NF), have gained considerable interest for their potential to improve performance while addressing solid waste management.

GP, which is obtained from post-consumer glass waste, is rich in reactive silica and displays pozzolanic activity. Several studies have confirmed that GP contributes to the enhancement of compressive strength and durability, particularly when used at low replacement levels [5–9]. Navaneetha, et al. [10] demonstrated that adding 5 % GP to sugarcane bagasse ash in ternary concrete improved compressive strength, thermal resistance, and chloride durability due to enhanced C–S–H gel formation and interfacial bonding. However, the same study reported reduced strength at higher GP contents, primarily due to dilution effects. Similarly, strength improvements with GP incorporation were reported by Shekhawat and Aggarwal [11]. Ramakrishnan et al. [12], Mithanthaya and Bhavanishankar Rao [13], Nassar and Abo [14], and Raydan et al. [15] observed increased tensile strength and improved crack resistance. However, GP contents exceeding 25 % have often been associated with increased water demand, reduced workability, and lower early-age strength [16–18].

RF, which is derived from recycled waste tires, has been extensively evaluated for its influence on the mechanical and durability properties of concrete. Letelier et al. [19] reported that RF improves workability, toughness, and energy absorption capacity. However, the inclusion of RF at higher replacement ratios has often been associated with reductions in compressive strength and modulus of elasticity due to its low specific gravity and poor interfacial bond with the cement matrix [20–22]. Despite these limitations, the use of RF has been shown to enhance ductility and increase post-crack load-bearing capacity in several studies [12–15].

Jia et al. [23] examined the durability of lightweight concrete incorporating waste glass powder (GP) and found that 20–30 % GP significantly improved corrosion resistance and microstructural densification under marine-like exposure conditions. These improvements were attributed to refined pore structures and enhanced steel passivation, although a slight reduction in early-age strength was observed. Similarly, Nia et al. [24] evaluated the replacement of silica fume with GP in ultra-high-performance concrete (UHPC) using Portland limestone cement and reported enhanced long-term compressive strength, improved permeability resistance, and better workability. These effects were primarily due to delayed pozzolanic activity, which led to the development of additional calcium silicate hydrate (C–S–H) and increased matrix density. Yuan et al. [25] further demonstrated that combining GP with eggshell powder improved frost resistance and compressive strength in high-strength concrete by refining the microstructure, reducing pore size, and promoting C–S–H formation. Tahwia et al. [26] showed that high-volume GP improved flowability and reduced permeability in UHPC by increasing pozzolanic reactivity and optimizing particle packing. Likewise, Su and Xu [27] confirmed that incorporating GP with rice husk ash enhanced compressive strength, cyclic loading resistance, and shear capacity, although a marginal increase in porosity was observed at higher replacement levels.

Despite extensive individual research on GP and RF, their combined application remains relatively underexplored. To address this, researchers have begun exploring their synergy, particularly in terms of mechanical behavior, durability, and microstructural refinement. Their individual effects on concrete performance differ significantly. GP enhances strength, durability, and matrix densification due to its pozzolanic activity and filler effect. RF contributes to toughness and energy dissipation, but often leads to a reduction in compressive strength and stiffness. Achieving a balanced use of both materials requires a careful mix design strategy, supported by robust optimization tools capable of analyzing the complex interactions between variables affecting fresh and hardened properties.

Response Surface Methodology (RSM) has emerged as a powerful statistical tool for optimizing concrete mixtures involving multiple interacting variables. It allows researchers to assess the effects of individual components and their interactions while reducing the number of experimental trials. Aldahdooh et al. [28–33] successfully used Central Composite Design (CCD)-based RSM (CCD-RSM) to optimize binder contents in ultra-high-performance fiber-reinforced cementitious composites, improving structural efficiency in retrofitting applications. Aldahdooh et al. [34] applied CCD-RSM to assess the effects of different types of plastic waste on concrete, validating the model predictions with experimental results. Almaawali et al. [35] used a customized Single-Factor RSM to optimize coarse recycled aggregate content in conventional concrete.

Other researchers have employed similar optimization frameworks to evaluate various recycled and industrial waste materials. Ali et al. [36] optimized mixtures containing waste foundry sand using CCD-RSM, while Ali et al. [37] applied the same design to optimize lightweight concrete with pumice. Hurtado-Alonso et al. [38] used RSM with desirability analysis for mixtures incorporating wind turbine blade waste and recycled aggregates. Abdellatief et al. [39] used a simplex centroid mixture design to optimize alkali-activated concrete made with recycled medical glass. Other researchers have also explored pozzolanic waste-based materials like pumice and rice straw ash in geopolymer systems to balance strength and durability, emphasizing sustainability [40]. Further studies by Habibi et al. [41] and Rezaei et al. [42], and Gopalakrishna and Dinakar [43] focused on optimizing nano-silica and supplementary cementitious materials in recycled aggregate concrete using CCD-RSM.

RSM has also been effectively applied in diverse sustainable concrete systems. Lovato et al. [44] optimized mechanical and durability properties in recycled aggregate concrete. Ahmed et al. [45] used RSM to evaluate the influence of polypropylene fibers and silica fume on recycled concrete performance. Zhang et al. [46] employed a Box–Behnken design to optimize porosity and compressive strength in pervious concrete. Aghajanzadeh et al. [47] applied RSM for the multi-objective optimization of alkali-activated slag concrete. Francioso et al. [48] used RSM to model thermal conductivity under various moisture and temperature conditions. Kareem et al. [49] optimized hybrid fiber-reinforced concrete containing waste steel and rubber fibers using Box–Behnken design, achieving improvements in strength, water resistance, and reduced CO_2 emissions. Matos et al. [50] applied CCD-RSM to optimize ternary mixtures of waste glass powder and limestone filler in white high-performance concrete, leading to improved mechanical properties and environmental benefits.

Although machine learning (ML) methods such as artificial neural networks (ANN) have shown high prediction accuracy in concrete research [51, 52], RSM remains more accessible and suitable for experimental optimization. As Ji et al. [53] and Zhao et al. [54] emphasized that ML approaches require large datasets and advanced computational infrastructure, which can limit practical application. Hammoudi et al. [55] compared RSM and ANN for strength prediction and concluded that RSM provided efficient and reliable results. Alahmari et al. [56] combined RSM and ML to identify optimal waste glass powder contents, improving strength and microstructure. Other studies such as those by Asif et al. [57–62], Ullah et al. [63], Miao et al. [64], and Ishaq et al. [65] further supported the high accuracy of ML models but acknowledged the complexity of implementation in small-scale experimental studies.

Only a limited number of studies have examined the combined use of GP and RF in concrete. Letelier et al. [19] explored cementitious mortars containing both crumb rubber and GP, and observed reductions in porosity and water absorption as well as improved thermal insulation, although strength losses persisted due to the inclusion of rubber. Mo et al. [66], Ramdani et al. [67], and Zhai et al. [68] showed that ultrafine GP improved the mechanical performance and microstructure of crumb rubber concrete by enhancing rubber–matrix bonding and refining pore characteristics. El Marzak et al. [69] and Song, Peng [78] demonstrated that combinations of GP with treated rubber or recycled aggregates led to increased strength and improved durability. Additional investigations by Katebi et al. [70], Chen et al. [71], Chen, Yang [81], and Mei et al. [72] supported the use of GP and RF in improving impact resistance, energy absorption, and structural performance in various concrete systems. Subramaniam [84] reviewed the effects of waste glass powder and crushed glass in pervious concrete and reported increased mechanical strength, permeability, and eco-efficiency. Mhaya et al. [73] and Parghi and Shahria Alam [74] studied lightweight and geopolymer mortars containing GP, RF, and supplementary binders. Mhaya et al. [73] reported that incorporating up to 15 % waste rubber powder (WRP) with glass powder and metakaolin achieved a 28-day compressive strength of 27.47 MPa with a 7.2 % reduction in density. Microstructural analysis showed improved pore refinement, increased gel formation (C–A–S–H and N–A–S–H), and a denser interfacial transition zone (ITZ). Although rubber inclusion raised water absorption slightly due to weak bonding, the pozzolanic activity of metakaolin compensated by enhancing matrix densification. These findings indicate the potential for improved durability and support the viability of combining GP and RF in lightweight, sustainable concrete systems.

Building on the above studies, this work aims to address the remaining research gap by integrating GP and RF into a unified optimization framework. Using CCD-RSM, the present study provides a holistic evaluation of their combined effects on multiple concrete properties. Despite the individual and limited combined studies on GP and RF in concrete, there remains a significant research gap in applying data-driven optimization techniques to balance their effects on multiple performance parameters. Letelier et al. [19] evaluated the combined use of GP and rubber in mortars, focusing on thermal insulation and microstructural behavior, without addressing structural-grade concrete or statistical optimization. Mo et al. [66] explored mechanical and shrinkage performance in rubberised glass concrete

with silica fume, but did not employ response surface modeling or explore broader performance interactions. Although Matos et al. [50] applied RSM to optimize ternary blends in high-performance white concrete using GP and limestone filler, they did not examine rubber aggregates or apply a Central Composite Design (CCD) approach. In contrast, the present study uniquely integrates GP and RF into structural concrete and utilizes CCD-based RSM to optimize a broader set of responses, including slump, compressive strength, splitting tensile strength, and modulus of elasticity. This integrated, model-driven framework offers a novel contribution to sustainable concrete mix design by providing statistically validated guidance for balancing mechanical performance and material circularity, offering practical applicability for industry adoption.

While the primary focus is on fresh and mechanical properties, the known microstructural densification effects of GP and the energy dissipation capacity of RF suggest potential benefits for long-term durability, such as reduced permeability and improved crack resistance, which merit future investigation.

Building on the identified research gap, this study aims to optimize the combined use of GP and RF in structural concrete by evaluating their effects on four key performance indicators: slump, compressive strength, splitting tensile strength, and modulus of elasticity. A Central Composite Design (CCD)-based Response Surface Methodology (RSM) is employed to systematically investigate the influence of GP and RF replacement levels, ranging from 0 % to 35 %. The objective is to identify sustainable concrete mixtures that achieve optimal performance while promoting material circularity, as illustrated in Figure 1.

2 Materials and methods

2.1 Materials

2.1.1 Portland cement

Ordinary Portland cement (OPC) CEM I (42.5 N) was used as the primary binder in this study. The cement was tested in accordance with the Egyptian Standard Specification ESS 4756-1/2007 [75] to ensure compliance with quality standards. The chemical analysis showed that the cement contains 63.2 % calcium oxide (CaO), 22.45 % silica (SiO_2), 4.8 % alumina (Al_2O_3), and 3.2 % iron oxide (Fe_2O_3), with a loss on ignition (LOI) of 2.25 %, confirming its suitability for concrete production (Table 1).

2.1.2 Glass powder (GP)

In this study, GP was used to partially replace OPC at 15 %, 25 %, and 35 % by weight. GP was produced from locally sourced post-consumer clear glass bottles through cleaning, drying, crushing, grinding, and sieving to achieve cement-like fineness (Figure 2). The chemical composition of GP was conducted to determine the composition of the produced GP, and the results are presented in Table 1. The analysis confirmed a high SiO_2 content (73.0 %) along with notable amounts of CaO (10.8 %) and Na_2O (11.4 %). X-ray diffraction (XRD) analysis confirmed the amorphous structure of GP, supporting its pozzolanic reactivity and suitability as a supplementary cementitious material.

2.1.3 Rubber fine aggregates

Rubber fine aggregates (RF) were used as a partial replacement for natural fine aggregates (NF) at levels of 15 %, 25 %, and 35 % by weight. RF was obtained from discarded tires, which were pre-processed to remove steel wires and contaminants, shredded, ground, and sieved through a 4.76 mm mesh to achieve uniform particle size (Figure 4). The physical properties of NF and RF are summarized in Table 2. RF exhibited a significantly lower specific gravity (1.06 g/cm^3) compared to NF (2.62 g/cm^3). While NF showed an absorption capacity of 0.82 %, RF displayed negligible water absorption due to its non-porous surface. A sieve analysis (Figure 5) confirmed that the particle size distribution of RF was comparable to that of NF. The surface texture of the raw RF material is shown in Figures 3–5.

2.2 Mix design and data analysis using RSM

The experimental program aimed to evaluate the influence of replacing cement with GP and NF with RF in concrete mixtures while maintaining essential mechanical and workability properties. This optimization uses RSM with a CCD approach implemented through Design-Expert® 6.0.7 software. The replacement levels of OPC with GP ([OPC-GP]%, X_1) and NF with RF ([NF-RF]%, X_2) were systematically varied at four levels (0 %, 15 %, 25 %, and 35 %), as outlined in Table 3. OPC with a constant content of 420 kg/m^3 was used, and the water-to-binder ratio was fixed at 0.4. Fine aggregates consisted of NF and RF. Crushed dolomite with a maximum size of 10 mm was used as the coarse aggregate. To maintain the desired workability without increasing the water content, a high-range water-reducing admixture

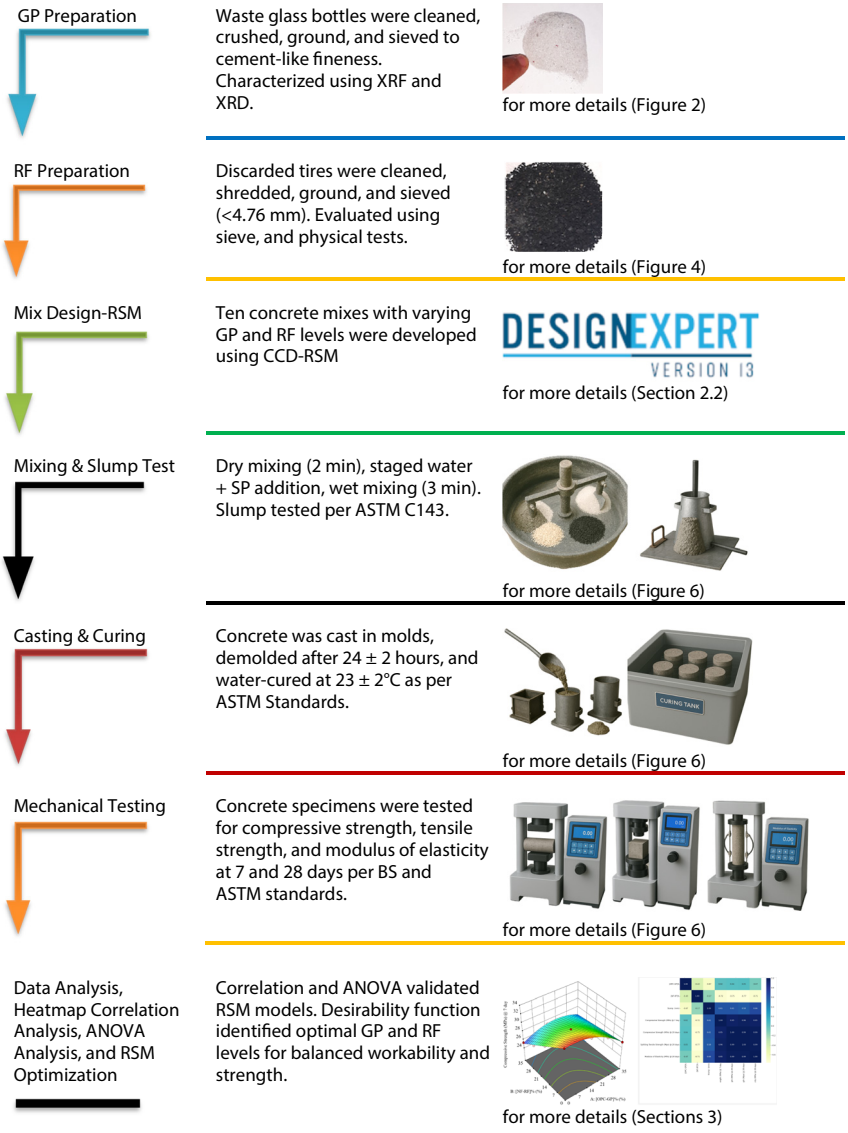

Figure 1: Methodological framework for sustainable concrete mix design incorporating GP and RF.

Table 1: Chemical composition of OPC and GP (by weight %).

Oxide	OPC (%)	GP (%)
SiO_2 – silicon dioxide	22.45	73.00
Al_2O_3 – aluminium oxide	4.80	1.80
Fe_2O_3 – ferric oxide	3.20	0.60
MgO – magnesium oxide	1.60	1.30
TiO_2 – titanium dioxide	–	0.03
CaO – calcium oxide	63.20	10.80
K_2O – potassium oxide	–	0.56
SO_3 – sulfur trioxide	2.50	–
Na_2O – sodium oxide	–	11.40
LOI – loss on ignition	2.25	0.60

(Type G), Sikament®R-2004, was incorporated at 2 % by weight of the binder. Sikament®R-2004 is a brown liquid with a density of 1.20 g/cm^3 at 20 °C, composed of modified synthetic dispersion. It complies with ASTM C496/C496M [76] and BS 5075-3: 1985 [77]. The admixture provides up to 20 % water reduction, enhances early and ultimate compressive strength, improves workability, and controls slump loss without causing segregation or adverse shrinkage. A constant water-to-binder ratio of 0.40 was maintained across all mixes, resulting in slump values between 80 and 93 mm, as presented in Table 3.

The experiment involved 10 concrete mixtures designed to examine relationships between the input factors (X_1 and X_2) and response variables, including slump (Y_1), compressive strength at 7 days (Y_2), compressive strength at 28 days (Y_3), splitting tensile strength at 28 days (Y_4), and modulus of elasticity at 28 days (Y_5). The responses were modeled using the quadratic equation:

Figure 2: Production process of GP.

Table 2: Physical properties of the aggregates.

Aggregate types	Specific gravity (g/cm^3)	Absorption (%)
Natural fine aggregates (NF)	2.62	0.82
Rubber fine aggregates (RF)	1.06	NA

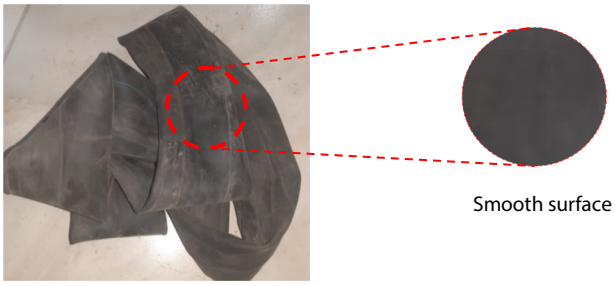

Figure 3: Raw rubber material showing a smooth surface texture before processing into rubber fine aggregates.

$$Y = \beta_0 + \sum_{i=1}^{k} \beta_i X_i + \sum_{i=1}^{k} \beta_{ii} X_i^2 + \sum_{i<j}^{k} \sum_{j}^{k} \beta_{ij} X_i X_j + e_i \quad (1)$$

Eq. (2) represents the matrix notation of the model:

$$Y = X\beta \pm \varepsilon \quad (2)$$

Here, Y represents the predicted responses, X is the coded input factors, β denotes the regression coefficients, and ε accounts for random errors. This quadratic model enabled accurate predictions of the responses and helped identify optimal replacement levels of GP and RF to achieve desirable concrete performance characteristics.

2.2.1 Analysis and optimization process

The optimization process involved evaluating the effects of [OPC-GP]% and [NF-RF]% on slump, compressive strength at 7 and 28 days, splitting tensile strength, and modulus of

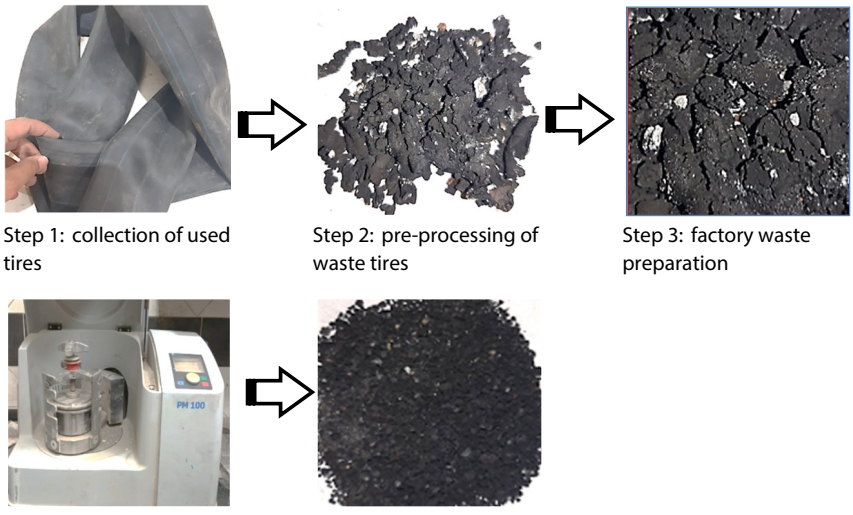

Figure 4: Production process of rubber fine aggregates (RF).

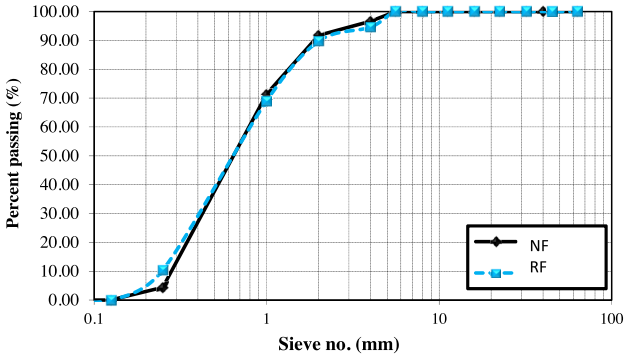

Figure 5: Sieve analysis of NF and RF.

elasticity at 28 days using ANOVA. Statistical significance was determined through R^2 values, *p*-values, *t*-tests, and diagnostic plots to ensure model adequacy. Each response was transformed into a desirability value (0–1) based on how well it met predefined performance criteria. Constraints were defined for all responses, and four optimization trials were conducted using varying goal settings to assess robustness (Table 7). A composite desirability index was used for multi-response optimization. Desirability plots (Figure 14) revealed that values near 1.0 consistently occurred when both [OPC-GP]% and [NF-RF]% exceeded 15 %. Based on this, Trial 1 was selected at 15 % GP and 15 % RF, achieving a desirability score of 1.000. Its optimality within the design space was confirmed through the ramp function graph (Figure 15). A comparison of all trials is provided in Table 9. The Trial 1 mix was then validated experimentally, with percentage errors for all responses remaining below 1.5 % (Table 10), confirming the model's predictive accuracy. This approach ensures a balanced mix in terms of mechanical performance and workability, supporting a systematic approach for optimizing sustainable concrete mixtures.

2.3 Sample preparation and testing procedure

In this study, saturated surface-dry CAs were mixed with dry OPC, GP (Figure 2), NF, and RF (Figure 4) in a pan mixer for 2 min. Then, 70–80 % of the total mixing water was added, followed by the remainder premixed with SP. Wet mixing continued for 3 min to ensure homogeneity. The complete mixing and testing procedure is illustrated in Figure 6. Immediately after mixing, the slump test was performed in accordance with ASTM C143/C143M [78], using a standard slump cone (300 mm height, 200 mm base diameter, 100 mm top diameter), and the results were recorded in millimeters (mm). The fresh concrete was cast into standard molds in two layers and compacted using a vibrating table or tamping rod. Specimens were demolded after 24 ± 2 h and cured in water at 23 ± 2 °C as per ASTM C192/C192M [79]. Mechanical properties were evaluated at 7 and 28 days. Compressive strength was tested on 150 mm cube specimens in accordance with BS 1881 [80], with three specimens per age (Table 4). The splitting tensile strength and modulus of elasticity were measured at 28 days using 150 × 300 mm cylindrical specimens, following ASTM C496/C496M-17 [76] and ASTM C469/C469M-14 [81], respectively. Modulus of elasticity results were further validated using Egyptian Standard Specifications ESS 203-2018 [37, 38]. Testing three specimens for each mechanical property ensured consistency and reliability in evaluating the concrete mixtures' workability and mechanical performance.

Table 3: CCD and mix proportions of concrete mixtures.

Mixture ID	CCD run #	Factors (CCD coded factors)		Mix proportions (kg/m^3)						
		X_1 [OPC-GP]%	X_2 [NF-FA]%	OPC	GP	NF	RF	CA	W	SP
GP0RF0	1	0 (−1.0)	0 (−1.0)	420	0	693.1	0	1,039.6	168	8.4
GP15RF0	2	15 (−0.143)	0 (−1.0)	357	15	589.14	103.97	1,039.6	168	8.4
GP25RF0	3	25 (0.429)	0 (−1.0)	315	25	519.83	173.28	1,039.6	168	8.4
GP35RF0	4	35 (1.0)	0 (−1.0)	273	35	450.52	242.59	1,039.6	168	8.4
GP0RF15	5	0 (−1.0)	15 (−0.143)	357	15	589.14	103.97	1,039.6	168	8.4
GP0RF25	6	0 (−1.0)	25 (0.429)	315	25	519.83	173.28	1,039.6	168	8.4
GP0RF35	7	0 (−1.0)	35 (1.0)	273	35	450.52	242.59	1,039.6	168	8.4
GP15RF15	8	15 (−0.143)	15 (−0.143)	357	15	589.14	103.97	1,039.6	168	8.4
GP15RF25	9	15 (−0.143)	25 (0.429)	315	25	519.83	173.28	1,039.6	168	8.4
GP15RF35	10	15 (−0.143)	35 (1.0)	273	35	450.52	242.59	1,039.6	168	8.4

[OPC] refers to the Portland cement, [GP] refers to the glass powder, [NF] refers to the natural fine, [RF] refers to the rubber fine aggregates, [CA] refers to the coarse aggregates, [W] refers to the water content, [SP] refers to the superplasticizer, [OPC-GP]% refers to the replacement level of OPC with GP, [NF-RF]% refers to the replacement level of NS with RF, [GP0RF0] refers to the control mixture with no replacement, and [GP15RF25] indicates a mixture with 15 % GP and 25 % RF.

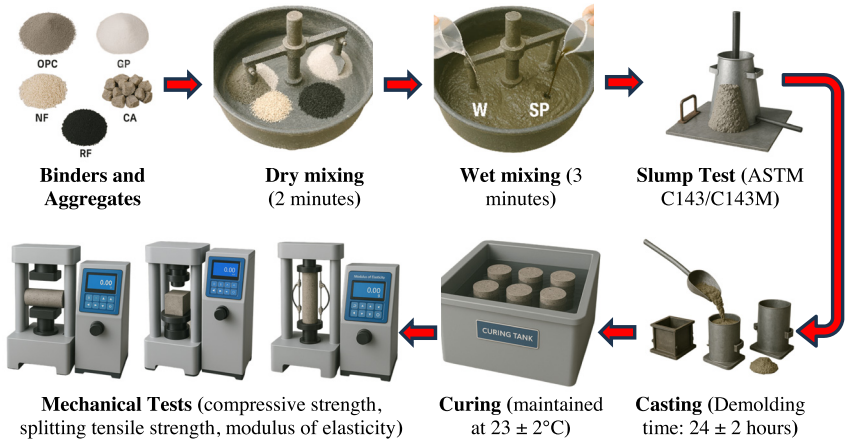

Figure 6: Concrete mixing and testing procedure.

Table 4: Summary of mechanical test methods and standards.

Property	Specimen type	Dimensions (diameter × height or side)	Age of testing (days)	Standard method
Compressive strength	Cube	150 mm × 150 mm × 150 mm	7 and 28	BS 1881 [80]
Splitting tensile strength	Cylinder	150 mm (D) × 300 mm (H)	28	ASTM C496/C496M-17 [76]
Modulus of elasticity	Cylinder	150 mm (D) × 300 mm (H)	28	ASTM C469/C469M-14 [81], ESS 203-2018 [37, 38]

3 Experimental results and discussions

This section presents the results of tests conducted on concrete mixtures, evaluating the influence of GP and RF as partial replacements for cement and natural fine aggregates, respectively, at levels of 15 %, 25 %, and 35 %. The responses include slump (Y_1), compressive strength at 7 days (Y_2), compressive strength at 28 days (Y_3), splitting tensile strength (Y_4), and modulus of elasticity (Y_5). Table 5 summarizes the results based on the factors X_1 ([OPC-GP]%) and X_2 ([NF-RF]%).

3.1 Slump test results

The workability of fresh concrete mixtures was evaluated using the standard slump test. Results are summarized in Table 5 and illustrated in Figure 7. Slump values ranged from

Table 5: Experimental results for each mixture.

Mixture ID	CCD run #	Factors		Responses (average values)				
		X_1 (%)	X_2 (%)	Y_1 (mm)	Y_2 (MPa)	Y_3 (MPa)	Y_4 (MPa)	Y_5 (MPa)
GP0RF0	1	0	0	95	32.89	40.37	5.5	26,221.3
GP15RF0	2	15	0	90	32.09	41.8	5.8	26,581.4
GP25RF0	3	25	0	85	30.28	39.6	5.3	25,896.5
GP35RF0	4	35	0	82	27.41	35.97	4.6	24,112.3
GP0RF15	5	0	15	95	29.5	38.6	5.08	25,724.5
GP0RF25	6	0	25	91	27.08	36.6	4.62	24,552.5
GP0RF35	7	0	35	85	25.3	33.7	4.21	23,734.1
GP15RF15	8	15	15	92	30.5	40.1	5.3	25,914.5
GP15RF25	9	15	25	89	28.54	37.4	4.8	24,827.7
GP15RF35	10	15	35	84	27.2	34.2	4.32	23,831.2

[GP0RF0] refers to the control mixture, [Y_1] refers to the slump (mm), [Y_2] refers to the compressive strength (MPa) at 7 days, [Y_3] refers to the compressive strength (MPa) at 28 days, [Y_4] refers to the splitting tensile strength (MPa) at 28 days, [Y_5] refers to the modulus of elasticity (MPa) at 28 days, [X_1] refers to the [OPC-GP]% and [X_2] refers to the [NF-RF]%.

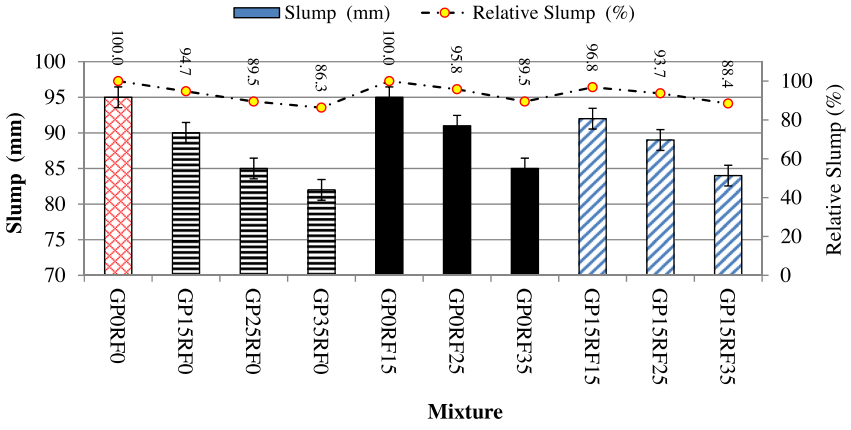

Figure 7: Influence of glass powder and rubber fine aggregate replacements on fresh concrete workability.

82 mm to 95 mm, all within the acceptable range for conventional concrete and below the 150 mm threshold typically associated with highly flowable mixes. Relative slump values, normalized to the control mixture (GP0RF0), ranged from 86.32 % to 100 %.

The control mixture (GP0RF0), composed entirely of OPC and NF, recorded the highest slump value of 95 mm. A gradual decline in slump was observed as the replacement level of OPC with GP increased. For example, slump decreased to 82 mm in the GP35RF0 mixture. This reduction is attributed to the high fineness and surface area of GP, which increase internal friction and water demand. As shown in Table 1, GP contains 73.0 % SiO_2 and has an amorphous structure, which enhances its pozzolanic reactivity while also increasing paste viscosity and reducing flowability. These observations are consistent with Sun et al. [82], who reported that high-surface-area materials reduce workability due to increased internal friction.

RF exhibited a more complex influence on slump. At a 15 % replacement level (GP0RF15), RF maintained the same slump as the control (95 mm), likely due to its smooth texture and elastic properties, which may improve particle movement at lower contents. However, higher RF contents (e.g., 25 % and 35 %) led to reduced slump values of 91 mm and 85 mm, respectively. According to Table 2, RF has a significantly lower specific gravity (1.06 g/cm^3) compared to NF (2.62 g/cm^3), and negligible water absorption. These properties reduce packing density and moisture retention, increasing internal resistance and decreasing workability. This behavior is consistent with the findings of Mehta and Gandhi [83] and Yu et al. [84], who demonstrated that higher-density aggregates improve flow by reducing internal friction, while lower-density materials impair workability.

Mixtures combining both GP and RF (e.g., GP15RF15 to GP15RF35) showed cumulative effects, with slump decreasing from 92 mm to 84 mm, indicating the combined impact of GP's high water demand and RF's low density and hydrophobic nature. Although a superplasticizer (SP), Sikament® R-2004, was included at a constant dosage of 2 % by binder weight in all mixtures, it primarily served to maintain workability across all mixes, rather than significantly improving flow, especially in mixtures with high GP and RF content.

In summary, although the inclusion of GP and RF influenced fresh concrete workability, no mixture exceeded a slump value of 95 mm. All mixtures remained within a consistent and controlled range suitable for casting and compaction. These results are in line with previous findings regarding the role of aggregate density, surface characteristics, and internal friction in determining concrete workability [41, 83, 84].

3.2 Mechanical properties

3.2.1 Compressive strength results

The compressive strength of all mixtures was evaluated at 7 and 28 days, as shown in Table 5 and illustrated in Figures 8 and 9. The reference mixture (GP0RF0), composed of 100 % OPC and NF, achieved 32.89 MPa at 7 days and 40.37 MPa at 28 days. It also recorded the highest slump value of 95 mm (Figure 7), indicating good workability and cohesiveness.

When OPC was partially replaced with GP (GP15RF0 to GP35RF0), compressive strength progressively declined with increasing replacement levels. At 28 days, strength decreased from 41.8 MPa (103.54 %) in GP15RF0 to 39.6 MPa (98.09 %) in GP25RF0 and 35.97 MPa (89.10 %) in GP35RF0. Slump values also declined, from 90 mm in GP15RF0 to 85 mm in GP25RF0 and 82 mm in GP35RF0 (Figure 7). These results suggest that the reduction in CaO content (10.8 % in GP vs. 63.2 % in OPC, Table 1) and the increased fineness of GP likely raised water demand and limited effective hydration at higher replacement levels. This interpretation is

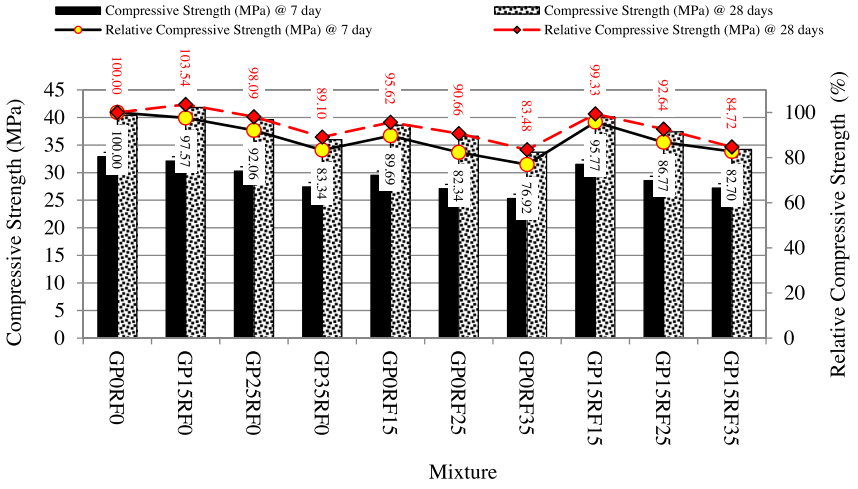

Figure 8: Compressive strength of concrete mixtures.

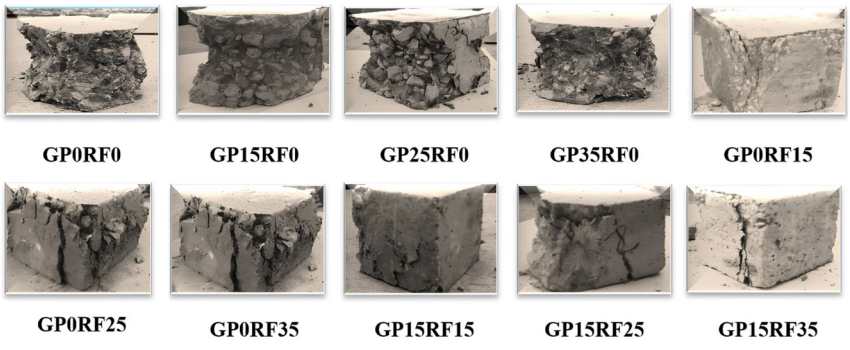

Figure 9: Failure behavior of concrete samples under compression.

consistent with findings by Matos et al. [50] and Nia et al. [24], who reported that high GP dosages can reduce strength due to cement dilution and increased water demand from fine particles, despite the pozzolanic benefits at moderate levels. The higher strength in GP15RF0 may be attributed to pozzolanic activity and improved particle packing at a moderate GP content, an effect also observed by Ramdani et al. [67] and Su and Xu [27], who highlighted the positive influence of GP on strength and densification when used in limited amounts. However, reduced flowability and higher internal friction at elevated GP levels may have hindered compaction efficiency, consistent with Mehta and Monteiro [85] and further supported by El Marzak et al. [69], who demonstrated that excess fines from SCMs and rubber can impair rheology and thus affect strength. This behavior is reflected in Figure 9, where GP35RF0 exhibited more brittle and irregular failure surfaces than GP15RF0.

Replacing NF with RF (GP0RF15 to GP0RF35) also resulted in reduced compressive strength. At 28 days, strength decreased from 38.6 MPa (95.62 %) in GP0RF15 to 36.6 MPa (90.66 %) in GP0RF25 and 33.7 MPa (83.48 %) in GP0RF35. Slump values also declined from 95 mm to 91 mm and 85 mm, respectively (Figure 7). According to Table 2, RF has a lower specific gravity (1.06 g/cm^3) and negligible water absorption compared to NF (2.62 g/cm^3, 0.82 %), which may reduce packing density and influence the aggregate–paste interaction. The elastic and smooth surface of RF (Figure 3) may also reduce mechanical interlock. These effects are consistent with the findings of Letelier et al. [19] and Mo et al. [66], who showed that rubber particles introduce internal voids, reduce stiffness, and weaken the interfacial transition zone (ITZ), ultimately leading to strength loss. As shown in Figure 9, GP0RF35 exhibited more extensive surface cracking than GP0RF15. These outcomes also align with Dils et al. [86] and Horszczaruk et al. [87], who reported that deformable rubber aggregates impair structural integrity by reducing packing efficiency and introducing high deformability zones.

Mixtures combining GP and RF (GP15RF15 to GP15RF35) exhibited similar trends. GP15RF15 achieved a 28-day strength of 40.1 MPa (99.33 %), close to the reference. Strength declined to 37.4 MPa (92.64 %) in GP15RF25 and 34.2 MPa (84.72 %) in GP15RF35. Slump values also decreased, from 92 mm in GP15RF15 to 89 mm and 84 mm, respectively (Figure 7). The performance of GP15RF15 indicates a balanced effect, where moderate GP and RF contents

maintained strength and workability. This result is in agreement with Ramdani et al. [67] and Mo et al. [66], who found that combining rubber and GP can offset strength losses caused by rubber alone due to the densifying and pozzolanic action of GP. However, increasing RF further resulted in lower strength and more fragmented fracture surfaces, as seen in Figure 9 for GP15RF35, reflecting a threshold beyond which the weakening effects of rubber dominate. This trend was also noted by El Marzak et al. [69].

In summary, compressive strength decreased with increasing GP and RF content, particularly beyond 15 %. This trend corresponded with lower slump values (Figure 7), indicating reduced flowability and compaction efficiency. The GP15RF15 mixture maintained strength comparable to the control with consistent failure behavior. These findings are in strong agreement with recent literature, including Letelier et al. [19], Mo et al. [66] and Matos et al. [50], which collectively confirm that moderate substitution levels of GP and RF can be optimized to retain structural performance, while excessive use negatively affects both workability and compressive strength due to microstructural inefficiencies.

3.2.2 Splitting tensile strength

The tensile strength results at 28 days are summarized in Table 6 and illustrated in Figure 10. The control mixture (GP0RF0) achieved the highest tensile strength of 5.5 MPa (100 %). Replacing cement with 15 % glass powder (GP15RF0) slightly improved the tensile strength to 5.8 MPa (105.45 %), which can be attributed to the filler effect of GP and its high SiO_2 content (73.0 %) (Table 1). These characteristics enhance matrix density and particle packing, thereby improving tensile behavior at lower replacement levels. This result aligns with the findings of Navaneetha et al. [10] and Matos et al. [50], who reported improved mechanical performance at moderate GP levels due to increased pozzolanic activity and refined pore structure. Similarly, Nia et al. [24] confirmed that GP enhances long-term strength through delayed pozzolanic reactions and additional C–S–H gel formation.

However, increasing the GP content to 25 % and 35 % led to reduced tensile strength values of 5.3 MPa (96.36 %) and 4.6 MPa (83.64 %), respectively. This decline is likely due to the higher water demand and delayed pozzolanic activity at elevated GP levels, which reduce the matrix's early-age strength. These trends are consistent with the dilution effects and strength reductions reported by Jia et al. [23] and Tahwia et al. [26] at higher GP levels.

When replacing NFs with RFs, tensile strength decreased progressively with increasing RF content. GP0RF15 achieved a tensile strength of 5.08 MPa (92.36 %), while GP0RF25 and GP0RF35 decreased further to 4.62 MPa (84.00 %) and 4.21 MPa (76.55 %), respectively. This reduction is primarily attributed to the lower specific gravity of RF (1.06 g/cm^3, Table 2), which weakens the interfacial bond between the cement paste and the aggregates, thereby reducing load transfer efficiency. Additionally, the irregular shape and elastic nature of RF particles increase void content and hinder stress distribution. These observations are consistent with findings by Letelier et al. [19], Mo et al. [66] and El Marzak et al. [69], who reported strength reductions in rubberized mixes due to poor interfacial bonding and increased porosity.

In combined replacement scenarios, the mixture GP15RF15 maintained a relatively high tensile strength of 5.35 MPa (97.27 %), suggesting a synergistic effect between moderate GP content and RF inclusion. This balance enhances matrix compactness while partially mitigating the negative impact of RF. Such synergy was also observed by Ramdani et al. [67] and Letelier et al. [19], who found that GP's pozzolanic and filler effects can compensate for the mechanical weaknesses introduced by rubber aggregates. However, as RF content increased further in mixes GP15RF25 and GP15RF35, tensile strength declined to 4.8 MPa (87.27 %) and 4.32 MPa (78.55 %), respectively. These reductions can be attributed to the lower stiffness, hydrophobic surface, and poor interfacial bonding of rubber particles, which negatively affect stress transfer and crack resistance.

The trends presented in Figure 10 confirm that tensile strength generally decreases as the replacement levels of both GP and RF increase. The reduction is more pronounced at higher RF levels due to its low density, deformability, and bond-disrupting characteristics. These findings underscore the importance of balancing GP and RF content to achieve an optimal trade-off between mechanical performance and sustainability. A moderate replacement level, such as 15 % GP and 15 % RF, proves effective in maintaining acceptable structural performance while promoting eco-efficiency.

3.2.3 Modulus of elasticity

The modulus of elasticity results at 28 days are presented in Figure 11. The control mixture (GP0RF0) recorded the highest modulus value of 26,221.3 MPa (100 %). When 15 % of cement was replaced with glass powder (GP15RF0), the modulus slightly increased to 26,581.4 MPa (101.37 %). This improvement can be attributed to the high SiO_2 content of the glass powder (73.0 %, Table 1), which enhances particle packing and contributes to matrix densification. Similar findings were reported by Matos et al. [50] and Nia et al. [24], who observed improved microstructure and stiffness in mixtures

Table 6: ANOVA results for response surface quadratic model parameters.

Response	Source	Sum of squares	df	Mean square	*F*-Value	*p*-Value	
Slump (mm)	Model	190.33	4	47.58	187.61	<0.0001	Significant
	x_1	30.03	1	30.03	118.41	0.0001	
	x_2	16.97	1	16.97	66.92	0.0004	
	x_1x_2	14.81	1	14.81	58.4	0.0006	
	x_2^2	33.21	1	33.21	130.95	<0.0001	
	Residual	1.27	5	0.2536			
	Cor total	191.6	9				
Compressive strength @ 7 days (MPa)	Model	51.8	4	12.95	209.49	<0.0001	Significant
	x_1	1.17	1	1.17	18.85	0.0074	
	x_2	10.16	1	10.16	164.35	<0.0001	
	x_1x_2	2.5	1	2.5	40.44	0.0014	
	x_1^2	2.91	1	2.91	47.02	0.001	
	Residual	0.3091	5	0.0618			
	Cor total	52.11	9				
Compressive strength @ 28 days (MPa)	Model	66.09	4	16.52	209.86	<0.0001	Significant
	x_1	13.38	1	13.38	169.88	<0.0001	
	x_2	59.19	1	59.19	751.75	<0.0001	
	x_1^2	16.1	1	16.1	204.51	<0.0001	
	x_2^2	2.99	1	2.99	38	0.0016	
	Residual	0.3937	5	0.0787			
	Cor total	66.48	9				
Splitting tensile strength @ 28 days (MPa)	Model	2.47	4	0.6167	168.84	<0.0001	Significant
	x_1	0.5833	1	0.5833	159.7	<0.0001	
	x_2	2.24	1	2.24	614.23	<0.0001	
	x_1^2	0.6466	1	0.6466	177.03	<0.0001	
	x_2^2	0.0237	1	0.0237	6.47	0.0516	
	Residual	0.0183	5	0.0037			
	Cor total	2.49	9				
Modulus of elasticity 28 days (MPa)	Model	9.82E+06	4	2.45E+06	93.39	<0.0001	Significant
	x_1	2.99E+06	1	2.99E+06	113.67	0.0001	
	x_2	8.77E+06	1	8.77E+06	333.82	<0.0001	
	x_1^2	2.56E+06	1	2.56E+06	97.45	0.0002	
	x_2^2	2.78E+05	1	2.78E+05	10.56	0.0227	
	Residual	1.31E+05	5	26,281.24			
	Cor total	9.95E+06	9				

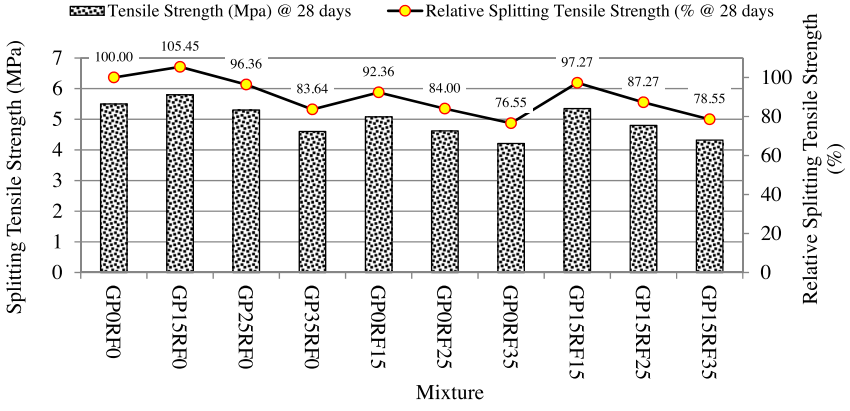

Figure 10: Splitting tensile strength of concrete mixtures.

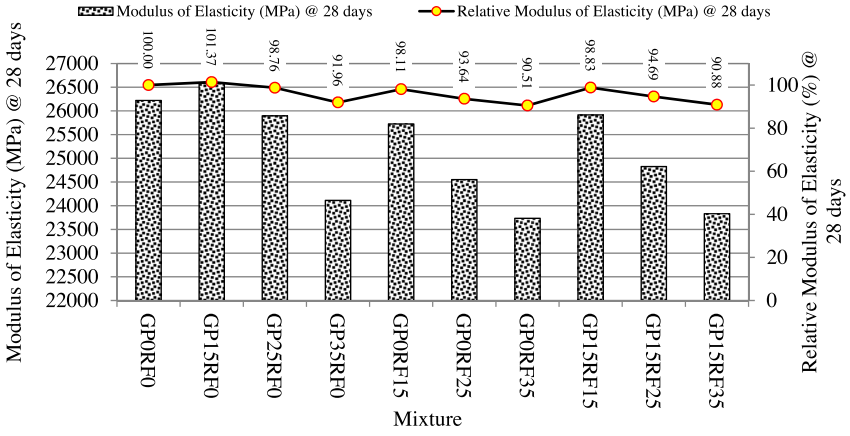

Figure 11: Modulus of elasticity of concrete mixtures.

incorporating moderate glass powder due to its pozzolanic activity and filler effect.

However, higher GP replacement levels (GP25RF0 and GP35RF0) resulted in reduced modulus values of 25,896.5 MPa (98.76 %) and 24,112.3 MPa (91.96 %), respectively. These reductions align with observations by Matos et al. [50] and Nia et al. [24], who reported that excessive GP content may lead to a dilution effect and delayed pozzolanic reaction, which in turn lowers stiffness and overall matrix integrity.

For rubber fine aggregate (RF) replacements, the modulus of elasticity consistently decreased with increasing RF content. The modulus values for GP0RF15, GP0RF25, and GP0RF35 were 25,724.5 MPa (98.11 %), 24,552.5 MPa (93.64 %), and 23,734.1 MPa (90.51 %), respectively. This trend is consistent with findings from Mo et al. [66] and El Marzak et al. [69], and Zhai et al. [68], who highlighted that rubber particles exhibit low stiffness, high deformability, and weak bonding at the interfacial transition zone (ITZ), all of which contribute to reduced elastic performance. The irregular surface and low specific gravity (1.06 g/cm^3, Table 2) of RF also disrupt the matrix continuity and contribute to stiffness loss.

In the case of combined GP and RF replacements, the mixture GP15RF15 demonstrated a modulus of 25,914.5 MPa (98.83 %), indicating a favorable synergy between moderate GP content and limited RF replacement. Ramdani et al. [67] and Letelier et al. [19] reported similar observations, where glass powder improved the microstructure and partially compensated for the adverse effects of rubber inclusion on mechanical performance.

However, higher RF contents in the combined mixes, such as GP15RF25 and GP15RF35, led to further reductions in modulus to 24,827.7 MPa (94.69 %) and 23,831.2 MPa (90.88 %), respectively. These findings are in line with those of Mo et al. [66] and El Marzak et al. [69], who confirmed that beyond certain thresholds, rubber content dominates the mechanical response, resulting in reduced stiffness and weaker structural behavior.

Overall, the trend in modulus of elasticity is consistent with the patterns observed in compressive and tensile strength, supporting the correlation between elastic stiffness and load-bearing capacity. The GP15RF15 mixture exhibited the most balanced performance, combining improved matrix densification from GP with an acceptable level of rigidity despite RF inclusion. These results emphasize the need to optimize the proportions of GP and RF to maintain mechanical performance while promoting sustainability in concrete production (as concluded in Section 3.2).

3.2.4 Heatmap correlation analysis and results

A heatmap correlation analysis was conducted to examine the relationships between [OPC-GP]%, [NF-RF]%, and key performance indicators: slump, compressive strength, splitting tensile strength, and modulus of elasticity. The correlation matrix, generated using Python and visualized with Seaborn (Figure 12), provided insights into how changes in material composition influence both fresh and hardened concrete properties.

The analysis showed a strong negative correlation between [OPC-GP]% and slump (r = −0.67), which aligns with the reduced workability observed in Section 3.1 as glass powder content increased. For instance, slump values decreased from 95 mm in GP0RF0 to 82 mm in GP35RF0. This reduction is attributed to the high surface area and fineness of the glass powder, which elevates water demand and internal friction. These findings are consistent with the conclusions of Sun et al. [82], who reported that high-surface-area materials lower workability due to increased internal resistance.

[OPC-GP]% exhibited minimal correlation with compressive strength at 7 days (r = 0.01), compressive strength at 28 days (r = 0.04), Splitting tensile strength at 28 days (r = 0.04), and modulus of elasticity at 28 days (r = −0.07). These weak associations suggest that the impact

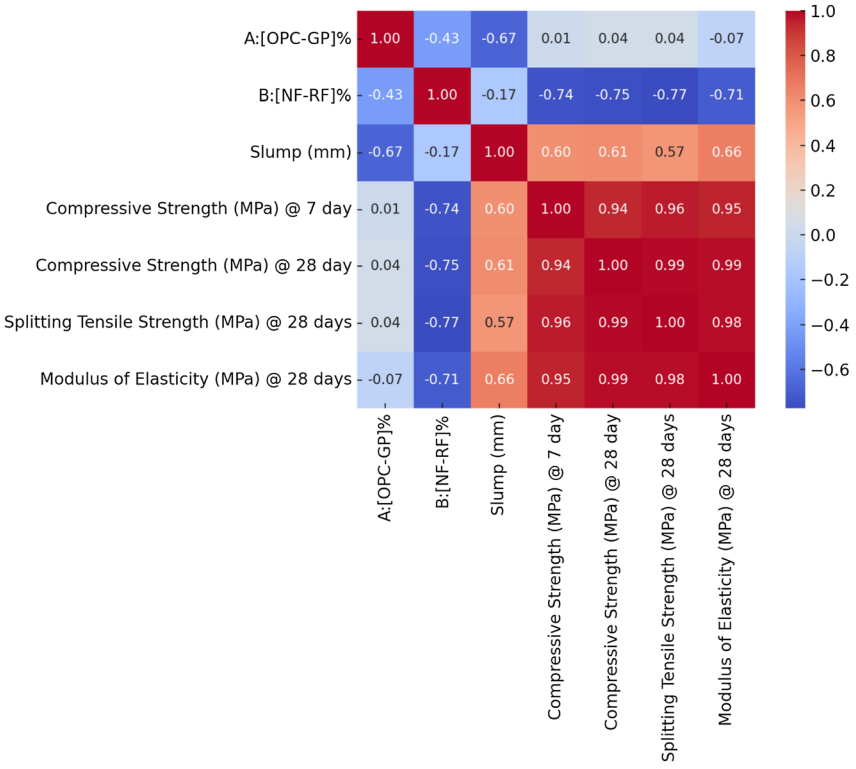

Figure 12: Correlation heatmap; factors and response metrics.

of glass powder on mechanical properties is nuanced, depending on the balance between pozzolanic reactivity and cement dilution. Conversely, [NF-RF]% displayed strong negative correlations with all mechanical properties: compressive strength at 7 days (r = −0.74), compressive strength at 28 days (r = −0.75), splitting tensile strength at 28 days (r = −0.77), and modulus of elasticity at 28 days (r = −0.71). These results are aligned with experimental outcomes discussed in Sections 3.2.1–3.2.3, where increasing rubber aggregate content reduced performance due to its low specific gravity, elastic nature, and limited bonding ability (see Table 2 and Figure 3).

Slump correlated positively with compressive strength at 7 days (r = 0.60), compressive strength at 28 days (r = 0.61), tensile strength at 28 days (r = 0.57), and modulus of elasticity at 28 days (r = 0.66). These moderate to strong correlations underscore the role of adequate workability in enhancing mechanical performance through improved compaction and reduced voids. For example, GP15RF0 and GP15RF15, with slump values of 90 mm and 92 mm, recorded high compressive strength values of 41.8 MPa and 40.1 MPa at 28 days, respectively.

Compressive strength at 7 days strongly correlated with compressive strength at 28 days (r = 0.94), tensile strength at 28 days (r = 0.96), and modulus of elasticity at 28 days (r = 0.95), indicating consistent strength progression. Similarly, compressive strength at 28 days correlated almost perfectly with splitting tensile strength (r = 0.99) and modulus of elasticity (r = 0.99), reinforcing its reliability as a predictor of other mechanical outcomes. Moreover, tensile strength and modulus of elasticity at 28 days showed a near-perfect correlation (r = 0.98), highlighting the intrinsic link between tensile behavior and material stiffness. This further supports the observations in Section 3.2.3 and emphasizes the importance of integrated mix design.

In summary, the correlation analysis confirms that moderate GP levels improve compressive strength and modulus of elasticity, likely due to enhanced pozzolanic action and particle packing. This is supported by Mhaya et al. [73], who showed that GP refines pore structure and densifies the matrix, reducing chloride penetration, enhancing corrosion resistance, and lowering capillary permeability in GP–rubber concretes. GP also promotes cohesive ITZ formation and C–S–H development, contributing to long-term durability. Conversely, higher RF content correlates with reduced mechanical performance due to its deformability, low specific gravity, and weak matrix bonding. However, RF's hydrophobic and elastic nature can mitigate crack propagation and water absorption, as evidenced by reduced surface erosion in GP–RF blends. These findings underscore the importance of optimizing GP and RF ratios to achieve both mechanical strength and durability, supporting sustainable concrete design.

3.3 RSM mathematical modeling and statistical insights

The relationships between process factors x_1 (replacement level of cement with glass powder [OPC-GP]%) and x_2 (replacement level of natural fine aggregates with rubber fine aggregates [NF-RF]%) and the responses (slump, compressive strength at 7 and 28 days, splitting tensile strength, and modulus of elasticity) were analyzed using RSM. Quadratic prediction models were developed using actual data, eliminating insignificant terms to enhance prediction accuracy. The predicted responses were modeled as quadratic functions of the factors, incorporating linear (x_1, x_2), interaction (x_1x_2), and quadratic (x_1^2, x_2^2) terms. The final prediction models for each response are expressed as follows:

$$\textbf{\textit{Slump}} = 95.13818 - 0.379266x_1 + 0.210915x_2 + 0.009532x_1x_2 - 0.014513x_2^2 \quad (3)$$

$$\textbf{\textit{Compressive strength @ 7 days (MPa)}} = 32.82507 + 0.044851x_1 - 0.220183x_2 + 0.005275x_1x_2 - 0.005727x_1^2 \quad (4)$$

$$\textbf{\textit{Compressive strength @ 28 days (MPa)}} = 40.53924 + 0.218163x_1 - 0.050989x_2 - 0.010004x_1^2 - 0.004355x_2^2 \quad (5)$$

$$\textbf{\textit{Splitting tesnile strength @ 28 days (MPa)}} = 5.54451 + 0.042607x_1 - 0.02605x_2 - 0.002005x_1^2 - 0.000387x_2^2 \quad (6)$$

$$\textbf{\textit{Modulus of elasticity @ 28 days (MPa)}} = 26338.36827 + 77.27164x_1 - 31.89193x_2 - 3.98995x_1^2 - 1.32629x_2^2 \quad (7)$$

3.3.1 ANOVA results and model significance

The statistical significance of the developed models was assessed using Analysis of Variance (ANOVA), as summarized in Table 6. All models were highly significant, with p-values less than 0.0001, confirming strong correlations between the process factors ([OPC-GP]% and [NF-RF]%) and the responses. For slump, the model showed an F-value of 187.61, with significant contributions from both linear and quadratic terms, especially [NF-RF]% (F = 130.95). The compressive strength at 7 days model achieved an F-value of 209.49, where the quadratic term of [OPC-GP]% had a dominant influence (F = 164.35). For compressive strength at 28 days, the model demonstrated an F-value of 209.86, with the linear term of [NF-RF]% exerting the most substantial effect (F = 751.75). Similarly, the splitting tensile strength at 28 days model recorded an F-value of 168.84, dominated by the linear and quadratic terms of [NF-RF]% (F = 614.23 and F = 177.03, respectively). The modulus of elasticity at 28 days achieved an F-value of 93.39, with significant contributions from the linear term of [NF-RF]% (F = 333.82) and the quadratic terms. The low residual mean square values across all models further confirm their precision and reliability in predicting the behavior of concrete mixtures with varying levels of glass powder and rubber fine aggregates.

3.3.2 Model validation

The accuracy and reliability of the models were validated using statistical metrics, including R^2, adjusted R^2, predicted R^2, and adequate precision, as summarized in Table 7. All responses exhibited R^2 values greater than 0.99, indicating that the models explain more than 99 % of the variability in the responses. The adjusted R^2 values were closely aligned with the R^2 values, confirming the models' robustness even after accounting for the number of predictors. The predicted R^2 values ranged between 0.93 and 0.98, demonstrating strong predictive accuracy for unseen data. Additionally, the adequate precision values for all responses exceeded 26, signifying an adequate signal-to-noise ratio, which ensures the models can effectively navigate the design space. The low coefficients of variation (C.V.%), ranging from 0.78 % to 2.5 %, further highlight the consistency and precision of the models. These results validate the models' reliability for predicting the slump, compressive strength, splitting tensile strength, and modulus of elasticity of concrete mixtures with varying levels of glass powder and rubber fine aggregates. It is important to note that while the developed RSM models show excellent predictive accuracy within the tested range (0–35 % replacement levels) for both factors, their application beyond this domain may be limited. RSM is inherently sensitive to the experimental range, and extrapolation should be approached with caution to avoid unreliable predictions.

3.3.3 Diagnostics and surface plots

The reliability of the RSM models was validated using diagnostic and response surface plots, as shown in Figure 13. The normal probability plots of studentized residuals

Table 7: Model validation for all responses.

Fit statistics	Slump	Compressive strength @ 7 days	Compressive strength @ 28 days	Splitting tensile strength @ 28 days	Modulus of elasticity @ 28 days
Std. dev.	0.504	0.25	0.28	0.06	162.11
Mean	88.8	29.08	37.83	4.95	25,139.6
C.V. %	0.57	0.86	0.74	1.22	0.64
R^2	0.99	0.99	0.99	0.99	0.99
Adj. R^2	0.99	0.99	0.99	0.99	0.98
Pred. R^2	0.98	0.98	0.97	0.95	0.93
Adeq. *P*.	37.28	43.83	41.03	36.83	26.19

[Std. Dev.] refers to the standard deviation; [Mean] refers to the average value; [C.V. %] refers to the coefficient of variation; [R^2] refers to the proportion of variance explained; [Adj. R^2] refers to the adjusted R^2 considering predictors; [Pred. R^2] refers to the predicted R^2; [Adeq *P*.] refers to the signal-to-noise ratio (Adeq precision).

(Figure 13-I) confirm normally distributed residuals, ensuring unbiased predictions. The predicted versus actual plots (Figure 13-II) demonstrate strong linear correlations, validating the models' accuracy. The perturbation plots (Figure 13-III) highlight the sensitivity of responses to changes in individual factors ([OPC-GP]% and [NF-RF]%), emphasizing the dominant influence of quadratic terms, particularly on compressive strength and modulus of elasticity.

The 3D surface plots (Figure 13-IV) illustrate the interaction effects of [OPC-GP]% and [NF-RF]% on key responses. For Slump, workability decreases with increasing [OPC-GP]% and [NF-RF]%, consistent with Section 3.2.1, where higher glass powder content increased water demand and rubber aggregates disrupted matrix continuity. For compressive strength, surface plots at 7 and 28 days show a parabolic trend: moderate [OPC-GP]% (15 %) enhances strength due to the pozzolanic activity of glass powder, while excessive [NF-RF]% reduces strength due to poor bonding and elastic deformability, aligning with Sections 3.2.1 and 3.2.3. Similarly, splitting tensile strength peaks at balanced levels of 15 % GP and 15 % RF (GP15RF15), achieving 5.35 MPa, as discussed in Section 3.2.2. For modulus of elasticity, surface plots mirror compressive strength trends, with peak values at 15 % GP and low RF content. Higher RF levels reduce stiffness due to their lower specific gravity and elastic nature, as highlighted in Section 3.2.3 and the correlation heatmap.

In summary, the 3D surface plots visualize the nonlinear interactions between [OPC-GP]% and [NF-RF]%, confirming earlier trends. Balanced replacement levels of 15 % GP and 15 % RF provide the best compromise between mechanical performance and workability, as supported by statistical models, experimental data, and correlation analysis.

3.3.4 Multiple response optimization

Multiple response optimization was performed using the desirability function to determine the optimal replacement levels of GP and RF for balanced concrete performance. The responses evaluated included slump, compressive strength at 7 and 28 days, splitting tensile strength, and modulus of elasticity at 28 days. Table 8 summarizes the constraints applied across four optimization trials, with goals set to either maintain values within specified ranges or maximize performance. All input factors and responses were assigned equal weights and high importance.

The desirability plots (Figure 14) show that values near 1.0 consistently occur when both [OPC-GP]% and [NF-RF]% exceed 15 %, establishing this threshold as a minimum for satisfying all performance criteria. Below this level, desirability declines sharply due to unmet targets. Based on this, Trial 1 was designed using 15 % GP and 15 % RF, marking the beginning of a stable optimal region. Trial 1 achieved a desirability score of 1.000, with strong performance across all responses: slump (91.49 mm), compressive strength at 28 days (39.82 MPa), splitting tensile strength (5.26 MPa), and modulus of elasticity (25,822.91 MPa). Trial 3 yielded a comparable mix (14.70 % GP and 15.61 % RF) with similar results. Trial 2 showed the highest strength and stiffness but excluded RF, reducing its sustainability contribution, with a desirability score of 0.987. Trial 4, which used the highest GP and RF content (25.19 % and 28.80 %), prioritized material substitution but resulted in lower mechanical performance and a desirability score of 0.770. A full comparison is provided in Table 9.

Considering both performance and sustainability, Trial 1 is recommended as the most balanced mix. The ramp function graph (Figure 15) illustrates its optimal position

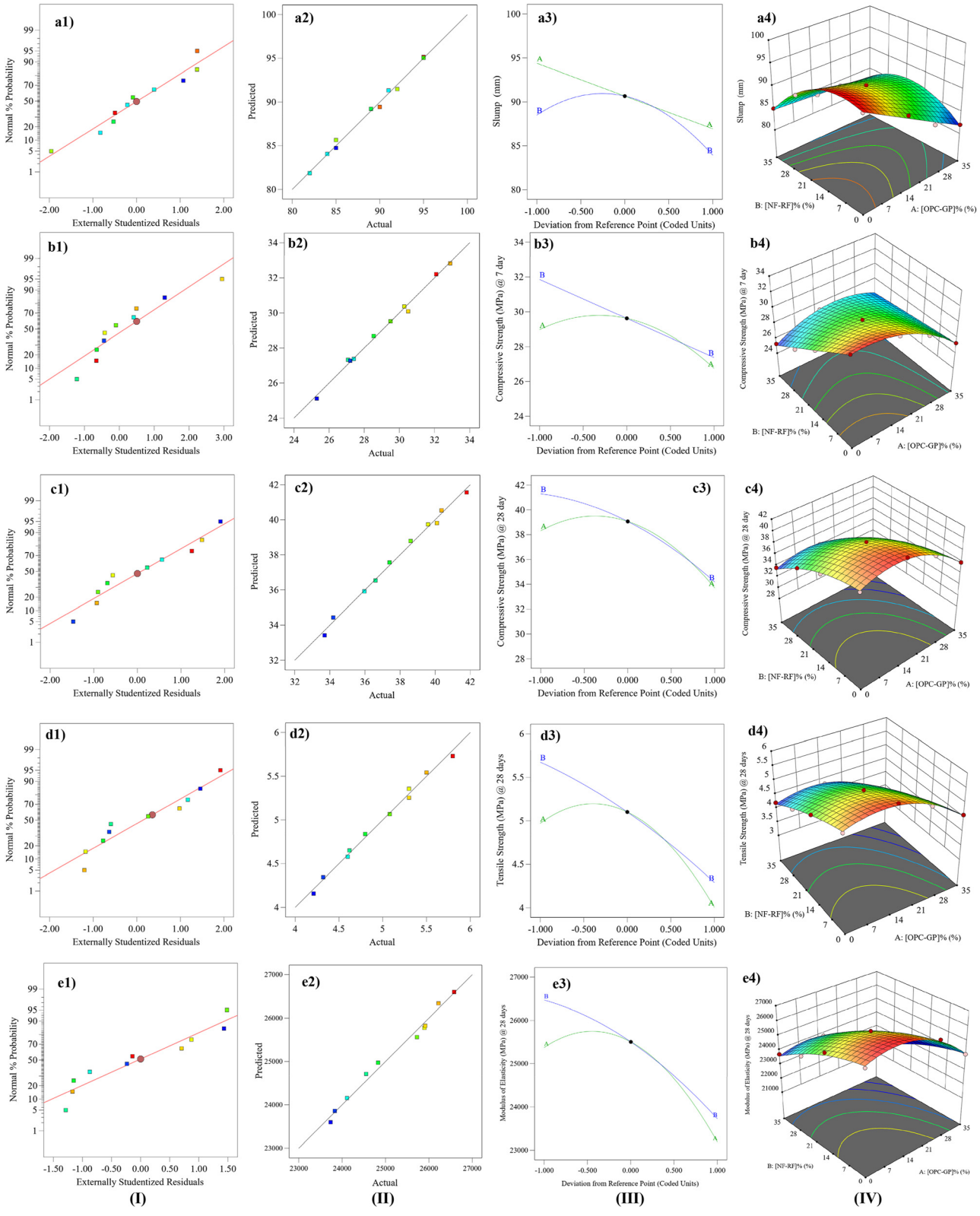

Figure 13: Diagnostics plots: (I) normal plot of the studentized residual, (II) predicted versus actual values plot, (III) perturbation plot, and (IV) 3D surface plot, for: (a) slump, (b) compressive strength at 7 days (c) compressive strength at 28 days, (d) splitting tensile strength at 28 days, (e) modulus of elasticity at 28 days.

Table 8: Optimization constraints for all trials using desirability function.

Name	Goal/Trial 1	Goal/Trial 2	Goal/Trial 3	Goal/Trial 4	Lower limit	Upper limit	Importance
A: [OPC-GP]%	Is in range	Is in range	Is in range	Maximize	Varies (0/15)	35	+++
B: [NF-RF]%	Is in range	Is in range	Is in range	Maximize	Varies (0/15)	35	+++
Slump	Is in range	Is in range	Is in range	Is in range	82	95	+++
Compressive strength @ 7 days	Is in range	Maximize	Is in range	Is in range	25.3	32.89	+++
Compressive strength @ 28 days	Is in range	Maximize	Is in range	Is in range	33.7	41.8	+++
Splitting tensile strength @ 28 days	Is in range	Maximize	Is in range	Is in range	4.21	5.8	+++
Modulus of elasticity @ 28 days	Is in range	Maximize	Is in range	Is in range	23,734.1	26,581.4	+++

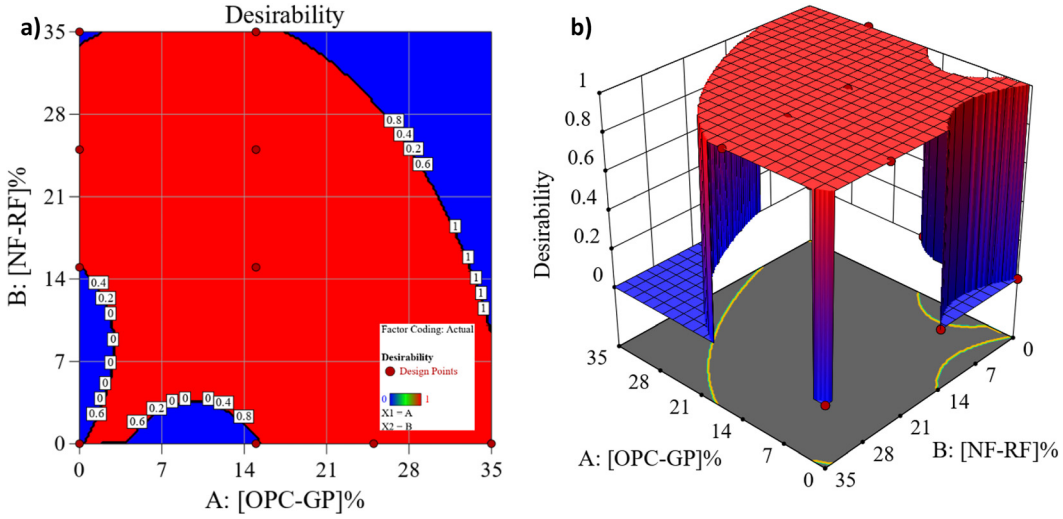

Figure 14: Desirability function plots showing optimal design region: (a) 2D contour and (b) 3D surface.

Table 9: Comparison of optimal mixture results across all trials.

Trial	[OPC-GP]%	[NF-RF]%	Slump (mm)	Compressive strength @ 7 days (MPa)	Compressive strength @ 28 days (MPa)	Tensile strength (MPa)	Modulus of elasticity (MPa)	Desirability	Status
Trial 1	15	15	91.49	30.09	39.82	5.26	25,822.91	1.000	Selected
Trial 2	9.174	0.0	91.66	32.76	41.70	5.77	26,711.45	0.987	
Trial 3	14.697	15.613	91.51	30.02	39.73	5.24	25,790.93	1.000	
Trial 4	25.191	28.802	86.54	27.81	34.61	4.27	23,734.10	0.770	

within the design space. For validation, the Trial 1 mix was experimentally tested and compared with model predictions (Table 10). Percentage errors for slump, compressive strength (7 and 28 days), splitting tensile strength, and modulus of elasticity were 0.55 %, 1.34 %, 0.70 %, 0.94 %, and 0.35 %, respectively. These low errors confirm the model's accuracy in predicting the performance of the optimized sustainable concrete mixture.

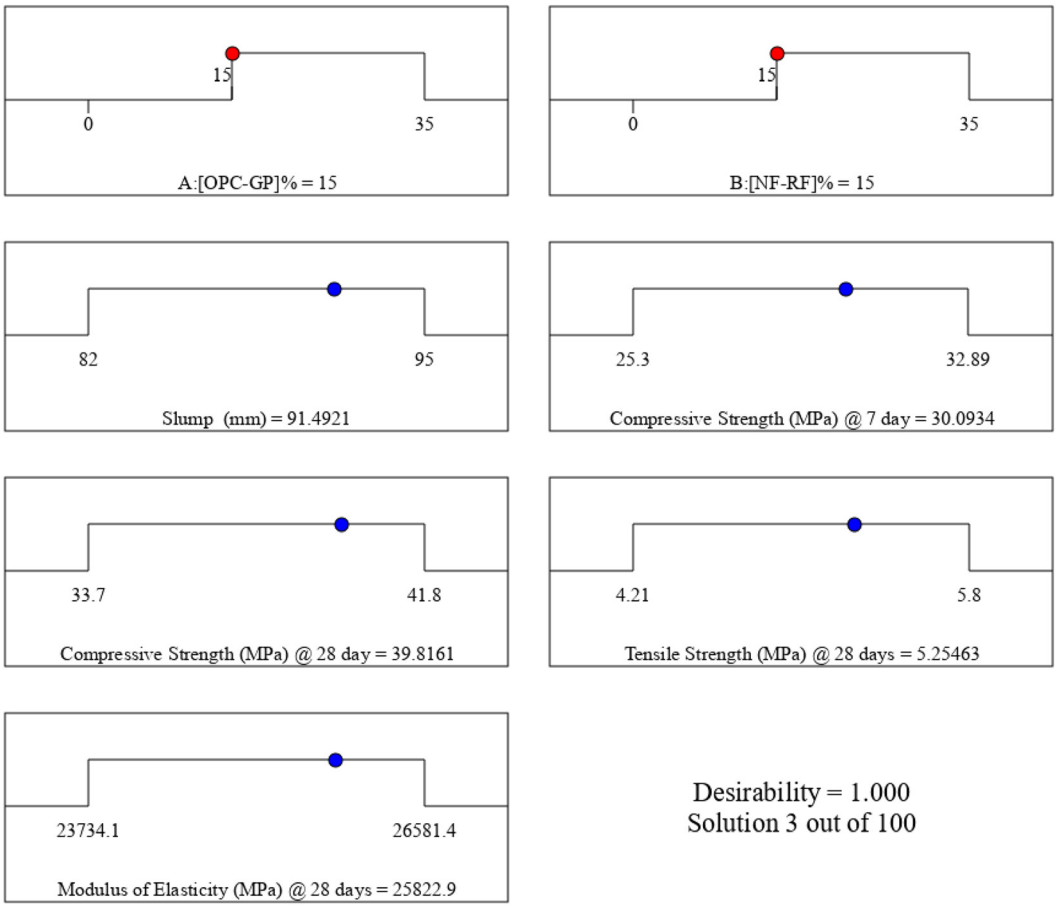

Figure 15: Ramp function graph for optimum responses (Trial 1) using desirability function.

Table 10: Comparison of predicted and experimental results for optimal mix (Trial 1) with corresponding percentage errors.

Response	Optimal solution			
	Predicted value	Actual value	Residual	% error
Slump (mm)	91.49	92	0.51	0.55 %
Compressive strength (MPa) @ 7 day	30.09	30.5	0.41	1.34 %
Compressive strength (MPa) @ 28 day	39.82	40.1	0.28	0.70 %
Tensile strength (MPa) @ 28 days	5.25	5.3	0.05	0.94 %
Modulus of elasticity (MPa) @ 28 days	25,823	25,914.5	91.5	0.35 %

4 Conclusions

This study investigated the combined use of glass powder (GP) and rubber fine aggregates (RF) as partial replacements for cement and natural fine aggregates (NF), respectively, in concrete. This study aligns with several Sustainable Development Goals (SDGs), no (9 and 11). Using a Central Composite Design (CCD) within the Response Surface Methodology (RSM) framework, 10 concrete mixtures were prepared with GP and RF replacement levels ranging from 0 % to 35 %. The mixtures were experimentally evaluated and statistically optimized. The key conclusions are as follows:

- Moderate GP replacement (15 %) enhanced mechanical properties due to its pozzolanic reactivity and filler effect, increasing matrix density. However, higher GP levels (25–35 %) reduced performance, likely due to increased water demand, dilution of cementitious content, and reduced early-age hydration.
- The inclusion of RF at 15 % maintained acceptable strength and workability, while higher RF levels (25–35 %) consistently reduced all mechanical properties. This reduction is attributed to RF's low specific gravity (1.06 g/cm^3) and elastic texture, which weakened bonding at the interfacial transition zone (ITZ) and increased internal voids.

- Correlation analysis revealed that compressive strength at 28 days strongly correlates with splitting tensile strength (r = 0.99) and modulus of elasticity (r = 0.99), indicating consistent mechanical performance. GP content showed weak positive correlations with strength ($r \approx 0.04$), whereas RF content showed strong negative correlations with compressive strength (r = −0.75), tensile strength (r = −0.77), and modulus of elasticity (r = −0.71). Slump was moderately correlated with all mechanical parameters (r = 0.57–0.66), underscoring the importance of fresh concrete workability in achieving reliable strength and stiffness.
- Multiple-response optimization using the desirability function identified GP15RF15 as the optimal mix, with a desirability score of 1.000. Predicted values were in close agreement with experimental results, with percentage errors below 1.35 % for all key responses, validating the model's accuracy and robustness.
- The optimal mix (GP15RF15) achieved a slump of 92 mm, compressive strength of 40.1 MPa, splitting tensile strength of 5.3 MPa, and modulus of elasticity of 25,914.5 MPa at 28 days, demonstrating performance comparable to the control mix (GP0RF0) while significantly improving sustainability.
- Fracture surface analysis indicated that mixes with high RF content exhibited more brittle and irregular cracking patterns. In contrast, GP15RF15 showed cohesive and uniform failure behavior, reflecting improved internal bonding and stress distribution.

This study presents a data-driven concrete mix incorporating 15 % glass powder (GP) and 15 % rubber fine aggregates (RF), offering a structurally viable and sustainable solution for pavements, non-prestressed structural components, and general infrastructure. The findings support circular economy principles by enabling the reuse of post-consumer waste without compromising mechanical performance. Although durability testing was beyond the scope of this study, the microstructural effects of GP and RF observed in the literature suggest potential improvements in durability-related aspects such as alkali–silica reaction resistance, permeability, and cracking behavior. These potential benefits, which are linked to the pozzolanic activity of GP and the energy absorption capacity of RF, warrant further investigation under long-term environmental exposure conditions.

Acknowledgments: The authors extend their appreciation to Prince Sattam bin Abdulaziz University for funding this research work through the project number (PSAU/2025/01/33470).

Funding information: This work was funded by the Prince Sattam bin Abdulaziz University through the project number (PSAU/2025/01/33470).

Author contribution: All authors have accepted responsibility for the entire content of this manuscript and approved its submission.

Conflict of interest: The authors state no conflict of interest.

Data availability statement: All data generated or analysed during this study are included in this published article.

References

1. Wittmann F. Structure of concrete with respect to crack formation. In: Fracture mechanics of concrete 1983:43–74.
2. Wittmann F. Crack formation and fracture energy of normal and high strength concrete. Sadhana 2002;27:413–23.
3. de Azevedo AR, Amin M, Hadzima-Nyarko M, Agwa IS, Zeyad AM, Tayeh BA, et al. Possibilities for the application of agro-industrial wastes in cementitious materials: a brief review of the Brazilian perspective. Clean Mater 2022;3:100040.
4. Hafez RDA, Tayeh BA, Abd-Al Ftah RO. Development and evaluation of green fired clay bricks using industrial and agricultural wastes. Case Stud Constr Mater 2022;17:e01391.
5. Bilgen G. Long-term compressive strength and microstructural appraisal of seawater, lime, and waste glass powder–treated clay soils. Arabian J Geosci 2022;15:1–18.
6. Ashiq SZ, Akbar A, Farooq K, Kazmi SMS, Munir MJ. Suitability assessment of marble, glass powders and poly-propylene fibers for improvement of siwalik clay. Sustainability 2022;14:2314.
7. Dong W, Li W, Tao Z. A comprehensive review on performance of cementitious and geopolymeric concretes with recycled waste glass as powder, sand or cullet. Resour Conserv Recycl 2021;172:105664.
8. Hakeem IY, Abd-Al Ftah RO, Tayeh BA, Hafez RDA. Eggshell as a fine aggregate replacer with silica fume and fly ash addition in concrete: a sustainable approach. Case Stud Constr Mater 2023;18:e01842.
9. Hamada H, Alattar A, Tayeh B, Yahaya F, Thomas B. Effect of recycled waste glass on the properties of high-performance concrete: a critical review. Case Stud Constr Mater 2022;17:e01149.
10. Navaneetha E, Rao PN, Bahurudeen A. Development of sustainable and durable ternary blended concrete using sugarcane bagasse ash and glass powder. Constr Build Mater 2025;466:140329.
11. Shekhawat BS, Aggarwal DV. Utilisation of waste glass powder in concrete – a literature review. Int J Innov Res Sci Eng Technol 2014;3.
12. Ramakrishnan K, Pugazhmani G, Sripragadeesh R, Muthu D, Venkatasubramanian C. Experimental study on the mechanical and durability properties of concrete with waste glass powder and ground granulated blast furnace slag as supplementary cementitious materials. Constr Build Mater 2017;156:739–49.
13. Mithanthaya I, Bhavanishankar Rao N. Effect of glass powder and GGBS on strength of fly ash based geopolymer concrete. Int J Eng Trends Technol 2015;19:66–71.
14. Nassar NE, Abo M. Effects of waste marble and glass powders on concrete properties and performance [Master's thesis]. North Cyprus: Eastern Mediterranean University (EMU)-Doğu Akdeniz Üniversitesi (DAÜ); 2020.
15. Raydan R, Khatib J, Jahami A, El Hamoui AK, Chamseddine F. Prediction of the mechanical strength of concrete containing glass powder as partial cement replacement material. Innov Infrastruct Solut 2022;7:311.

16. Orouji M, Zahrai SM, Najaf E. Effect of glass powder & polypropylene fibers on compressive and flexural strengths, toughness and ductility of concrete: an environmental approach. In: Structures. Elsevier; 2021: 4616–28 pp.
17. Niang A, Roy N, Tagnit-Hamou A. Structural behavior of concrete incorporating glass powder used in reinforced concrete columns. J Struct Eng 2015;141:B4014007.
18. Li G, Stubblefield MA, Garrick G, Eggers J, Abadie C, Huang B. Development of waste tire modified concrete. Cement Concr Res 2004;34:2283–9.
19. Letelier V, Bustamante M, Olave B, Martínez C, Ortega JM. Properties of mortars containing crumb rubber and glass powder. Dev Built Environ 2023;14:100131.
20. Geng C, Wu X, Yao X, Wang C, Mei Z, Jiang T. Reusing waste glass powder to improve the strength stability of cement at HTHP. J Petrol Sci Eng 2022;213:110394.
21. Siad H, Lachemi M, Sahmaran M, Mesbah HA, Hossain KMA. Use of recycled glass powder to improve the performance properties of high volume fly ash-engineered cementitious composites. Constr Build Mater 2018;163:53–62.
22. Shoji D, He Z, Zhang D, Li VC. The greening of engineered cementitious composites (ECC): a review. Constr Build Mater 2022;327:126701.
23. Jia B, Peng L, Zhao Y. Recycling waste glass powder in lightweight aggregate concrete: towards lightweight, sustainable and durable marine engineering structures. Constr Build Mater 2025;472:140690.
24. Nia SB, Nyland A, Wivast J, Kioumarsi M, Shafei B. Investigations of Portland limestone cement and waste glass powder for sustainable ultra-high performance concrete. Case Stud Constr Mater 2025;22: e04425.
25. Yuan X, Zhou Y, Yang H, Dai M, Liu F, Yan S. Anti-freezing performance and micro deterioration model for high-strength concrete modified with waste glass powder and eggshell particles. Constr Build Mater 2025;472:140832.
26. Tahwia AM, Essam A, Tayeh BA, Elrahman MA. Enhancing sustainability of ultra-high performance concrete utilizing high-volume waste glass powder. Case Stud Constr Mater 2022;17:e01648.
27. Su Q, Xu J. Mechanical properties of rice husk ash and glass powder concrete: experimental and mesoscopic studies. J Build Eng 2024;95: 110278.
28. Aldahdooh M, Alnuaimi A, Jamrah A, Bunnori NM, Johari MM, Martini M. GUSMRC – from concept to structural application. De Gruyter 2017;7: 133–46.
29. Aldahdooh M, Bunnori NM, Johari MM. Influence of palm oil fuel ash on ultimate flexural and uniaxial tensile strength of green ultra-high performance fiber reinforced cementitious composites. Mater Des 2014;54:694–701.
30. Aldahdooh MAA. Development of pofa-based green ultra-high performance fiber reinforced cementitious composites as retrofitting material [Doctoral dissertation]. Malaysia: Universiti sains Malaysia; 2014.
31. Aldahdooh MAA. Utilization of by-product materials in ultra high-performance fiber reinforced cementitious composites. In: Cement based materials. IntechOpen; 2018:113 p.
32. Aldahdooh MAA, Muhamad Bunnori N, Megat Johari MA. Evaluation of ultra-high-performance-fiber reinforced concrete binder content using the response surface method. Mater Des 2013;52:957–65.
33. Aldahdooh MAA, Muhamad Bunnori N, Megat Johari MA. Development of green ultra-high performance fiber reinforced concrete containing ultrafine palm oil fuel ash. Constr Build Mater 2013;48:379–89.
34. Aldahdooh MAA, Jamrah A, Alnuaimi A, Martini MI, Ahmed MSR, Ahmed ASR. Influence of various plastics-waste aggregates on properties of normal concrete. J Build Eng 2018;17:13–22.
35. Almaawali S, Aldahdooh MAA, Alnaamani SAM, Ibrahim NT, Ng CA. Optimization of sustainable concrete incorporating coarse recycled aggregate using a customized single-factor response surface methodology (CSFRSM) approach. Discov Civ Eng 2025;2:36.
36. Ali M, Khan MI, Masood F, Alsulami BT, Bouallegue B, Nawaz R, et al. Central composite design application in the optimization of the effect of waste foundry sand on concrete properties using RSM. Structures 2022;46:1581–94.
37. Ali M, Kumar A, Yvaz A, Salah B. Central composite design application in the optimization of the effect of pumice stone on lightweight concrete properties using RSM. Case Stud Constr Mater 2023;18:e01958.
38. Hurtado-Alonso N, Manso-Morato J, Revilla-Cuesta V, Skaf M. Strength-based RSM optimization of concrete containing coarse recycled concrete aggregate and raw-crushed wind-turbine blade. Compos Struct 2025;356:118895.
39. Abdellatief M, Adel B, Alanazi H, Tawfik TA. Multiscale optimization analysis of high strength alkali-activated concrete containing waste medical glass under exposure to carbonation and elevated temperatures. Dev Built Environ 2024;19:100492.
40. Elfadaly E, Othman AM, Aly MH, Elgarhy WA, Abdellatief M. Assessing performance and environmental benefits of high-performance geopolymer mortar incorporating pumice and rice straw ash. Sustain Chem Pharm 2025;44:101918.
41. Habibi A, Ramezanianpour AM, Mahdikhani M, Bamshad O. RSM-based evaluation of mechanical and durability properties of recycled aggregate concrete containing GGBFS and silica fume. Constr Build Mater 2021;270:121431.
42. Rezaei F, Memarzadeh A, Davoodi M-R, Dashab M-A, Nematzadeh M. Mechanical features and durability of concrete incorporating recycled coarse aggregate and nano-silica: experimental study, prediction, and optimization. J Build Eng 2023;73:106715.
43. Gopalakrishna B, Dinakar P. An innovative approach to fly ash-based geopolymer concrete mix design: utilizing 100 % recycled aggregates. Structures 2024;66:106819.
44. Lovato PS, Possan E, Dal Molin DCC, Masuero ÂB, Ribeiro JLD. Modeling of mechanical properties and durability of recycled aggregate concretes. Constr Build Mater 2012;26:437–47.
45. Ahmed TW, Ali AAM, Zidan RS. Properties of high strength polypropylene fiber concrete containing recycled aggregate. Constr Build Mater 2020;241:118010.
46. Zhang Q, Feng X, Chen X, Lu K. Mix design for recycled aggregate pervious concrete based on response surface methodology. Constr Build Mater 2020;259:119776.
47. Aghajanzadeh I, Ramezanianpour AM, Amani A, Habibi A. Mixture optimization of alkali activated slag concrete containing recycled concrete aggregates and silica fume using response surface method. Constr Build Mater 2024;425:135928.
48. Francioso V, Moro C, Velay-Lizancos M. Effect of recycled concrete aggregate (RCA) on mortar's thermal conductivity susceptibility to variations of moisture content and ambient temperature. J Build Eng 2021;43:103208.
49. Kareem MA, Ajadi EO, Fadipe OO, Ishola K, Olawuyi OA, Ayanlere SA, et al. Sustainability-driven application of waste steel and tyre rubber fibres as reinforcement in concrete: an optimization study using response surface methodology. Next Mater 2025;7:100345.

50. Matos AM, Milheiro-Oliveira P, Pimentel M. Eco-efficient high performance white concrete incorporating waste glass powder. Constr Build Mater 2024;411:134556.
51. Joseph HS, Pachiappan T, Avudaiappan S, Guindos P. Prediction of the mechanical properties of concrete incorporating simultaneous utilization of fine and coarse recycled aggregate. Rev. constr. 2023;22:178–91.
52. Chiranjeevi K, Kumar DH, Srinivasa AS, Ravi Shankar A. Optimisation of recycled concrete aggregates for cement-treated bases by response surface method. Int J Pavement Eng 2023;24:2179051.
53. Ji Y, Wang D, Wang J. Study of recycled concrete properties and prediction using machine learning methods. J Build Eng 2024;94: 110067.
54. Zhao Z, Liu Y, Lu Y, Ji C, Lin C, Yao L, et al. Prediction of properties of recycled aggregate concrete using machine learning models: a critical review. J Build Eng 2024;90:109516.
55. Hammoudi A, Moussaceb K, Belebchouche C, Dahmoune F. Comparison of artificial neural network (ANN) and response surface methodology (RSM) prediction in compressive strength of recycled concrete aggregates. Constr Build Mater 2019;209:425–36.
56. Alahmari TS, Kabbo MKI, Sobuz MHR, Rahman SMA. Experimental assessment and hybrid machine learning-based feature importance analysis with the optimization of compressive strength of waste glass powder-modified concrete. Mater Today Commun 2025;44:112081.
57. Asif U, Javed MF. Optimizing plastic waste inclusion in paver blocks: balancing performance, environmental impact, and cost through LCA and economic analysis. J Clean Prod 2024;478:143901.
58. Asif U, Javed MF, Abuhussain M, Ali M, Khan WA, Mohamed A. Predicting the mechanical properties of plastic concrete: an optimization method by using genetic programming and ensemble learners. Case Stud Constr Mater 2024;20:e03135.
59. Asif U, Javed MF, Alsekait DM, AbdElminaam DS, Alabduljabbar H. Toward sustainability: integrating experimental study and data-driven modeling for eco-friendly paver blocks containing plastic waste. Rev Adv Mater Sci 2024;63. https://doi.org/10.1515/rams-2024-0051.
60. Asif U, Javed MF, Alyami M, Hammad AWA. Performance evaluation of concrete made with plastic waste using multi-expression programming. Mater Today Commun 2024;39:108789.
61. Asif U, Memon SA. Interpretable predictive modeling, sustainability assessment, and cost analysis of cement-based composite containing secondary raw materials. Constr Build Mater 2025;473:140924.
62. Asif U, Memon SA, Javed MF, Kim J. Predictive modeling and experimental validation for assessing the mechanical properties of cementitious composites made with silica fume and ground granulated blast furnace slag. Buildings 2024;14:1091.
63. Ullah W, Bin Inqiad W, Ayub B, Khan MS, Javed MF. An explainable machine learning (XML) approach to determine strength of glass powder concrete. Mater Today Commun 2025;45:112181.
64. Miao X, Chen B, Zhao Y. Prediction of compressive strength of glass powder concrete based on artificial intelligence. J Build Eng 2024;91: 109377.
65. Ishaq MB, Mohammed AS, Mohammed AA. Novel exploration of chemical compounds in mono-variate, Bi-variate, and multi-variate scenarios of waste glass powder as a cement replacement in concrete. Sustain Chem Pharm 2025;43:101894.
66. Mo J, Tian S, Ren F, Ho JCM. Improving the performance of crumb rubber concrete using waste ultrafine glass powder. Structures 2024; 70:107775.
67. Ramdani S, Guettala A, Benmalek ML, Aguiar JB. Physical and mechanical performance of concrete made with waste rubber aggregate, glass powder and silica sand powder. J Build Eng 2019;21:302–11.
68. Zhai S, Hu J, Hai R, Cui L, Yang L, Zhang J, et al. Investigation on the durability performance and mechanism analysis of modified crumb rubber concrete. Constr Build Mater 2025;471:140746.
69. El Marzak M, Karim Serroukh H, Benaicha M, Jalbaud O, Hafidi Alaoui A, Burtschell Y. Rheological and mechanical analysis of self-compacting concrete incorporating rubber aggregates. Case Stud Constr Mater 2025;22:e04564.
70. Katebi A, Asadollahfardi G, Salehi A, Ahmadi G, Soleymani-tushmanlo A. Investigation of the properties of self-compacting concrete using treated rubber powder, polypropylene fibers, and wash water. Case Stud Constr Mater 2025;22:e04443.
71. Chen L, Yang F, Hong Y, Feng W, Li X. Dynamic mechanical properties and failure mechanism of sustainable lightweight aggregate rubber concrete. J Mater Res Technol 2025;35:1982–95.
72. Mei X, Li J, Zhang J, Cui Z, Zhou J, Li C. Predicting energy absorption characteristic of rubber concrete materials. Constr Build Mater 2025; 465:140248.
73. Mhaya AM, Shahidan S, Goel A, Huseien GF. Effect of metakaolin content and shape design on strength performance of lightweight rubberized geopolymer mortars incorporated slag-waste glass powders. Constr Build Mater 2024;432:136500.
74. Parghi A, Shahria Alam M. Physical and mechanical properties of cementitious composites containing recycled glass powder (RGP) and styrene butadiene rubber (SBR). Constr Build Mater 2016;104:34–43.
75. E. No, 4756-1, Egyptian Standard Specification, 2007, Portland Cement 2013.
76. ASTM C496/C496M, Standard Test Method for Splitting Tensile Strength of Cylindrical Concrete Specimens, ASTM International, West Conshohocken, PA 19428-2959, United States, 1996.
77. BS 5075-3: 1985, Concrete admixtures – Part 3: Specification for superplasticizing admixtures, University of Sheffield, BRITISH STANDARD, UK.
78. ASTM: C143/C143M, Standard Test Method for Slump of Hydraulic-Cement Concrete, ASTM International, West Conshohocken, PA 19428-2959, United States, 1998.
79. ASTM C192/C192M-19a, Standard Practice for Making and Curing Concrete Test Specimens in the Laboratory., ASTM International, West Conshohocken, PA.
80. BS 1881-108:98, method of making test cubes from fresh concrete licensed, British Standards Institution, London, UK, 11 pp.
81. C. Astm, 469. Standard test method for static modulus of elasticity and poissons ratio of concrete in compression, ASTM Standards, American Society for Testing and Materials, Pennsylvania; 2002.
82. Sun M, Li J, Zhang H, Chi R, Pang B, Cao W, et al. Effect of relative density and grain size on the internal flow field during the ballistic penetration of sand. Int. J. Impact Eng. 2024;185:104859.
83. Mehta P, Gandhi A. Influence of particle size gradation and relative density on shear parameters for cohesionless soil. Int J Adv Res Innov Ideas Educ 2016;2:869–78.
84. Yu X, Wang D, Chen Z, He S, Li H, Xu YJPT. Experimental investigation on rheological behavior of dry granular mixtures based on direct measurement of basal friction. Powder Technol 2024;438:119674.
85. Mehta PK, Monteiro P. Concrete: microstructure, properties, and materials. New York: McGraw-Hill Education; 2014.
86. Dils J, Boel V, De Schutter GJC, Materials B. Influence of cement type and mixing pressure on air content, rheology and mechanical properties of UHPC. Constr. Build. Mater. 2013;41:455–63.
87. Horszczaruk E, Brzozowski PJC. Investigation of gamma ray shielding efficiency and physicomechanical performances of heavyweight concrete subjected to high temperature. Constr. Build. Mater. 2019;195:574–82.